ADVANCED HEALTHCARE MATERIALS
www.advhealthmat.de

Hemagglutinin Functionalized Liposomal Vaccines Enhance Germinal Center and Follicular Helper T Cell Immunity

Mai N. Vu, Hannah G. Kelly, Hyon-Xhi Tan, Jennifer A. Juno, Robyn Esterbauer, Thomas P. Davis, Nghia P. Truong, Adam K. Wheatley,* and Stephen J. Kent**

Despite remarkable successes of immunization in protecting public health, safe and effective vaccines against a number of life-threatening pathogens such as HIV, ebola, influenza, and SARS-CoV-2 remain urgently needed. Subunit vaccines can avoid potential toxicity associated with traditional whole virion-inactivated and live-attenuated vaccines; however, the immunogenicity of subunit vaccines is often poor. A facile method is here reported to produce lipid nanoparticle subunit vaccines that exhibit high immunogenicity and elicit protection against influenza virus. Influenza hemagglutinin (HA) immunogens are functionalized on the surface of liposomes via stable metal chelation chemistry, using a scalable advanced microfluidic mixing technology (NanoAssemblr). Immunization of mice with HA-liposomes elicits increased serum antibody titers and superior protection against highly pathogenic virus challenge compared with free HA protein. HA-liposomal vaccines display enhanced antigen deposition into germinal centers within the draining lymph nodes, driving increased HA-specific B cell, and follicular helper T cell responses. This work provides mechanistic insights into highly protective HA-liposome vaccines and informs the rational design and rapid production of next generation nanoparticle subunit vaccines.

1. Introduction

Current influenza vaccines including live attenuated viruses, inactivated split virions, and recombinant proteins, all suffer from suboptimal immunity of limited breadth that rapidly wanes. Nanoparticle (NP) vaccines, where subunit antigens are arranged in a particulate platform, more closely mimic native viral structures and have a favorable profile of safety and potent immunogenicity.[1] Several particle scaffolds for delivering subunit influenza antigens have been reported, primarily studying delivering hemagglutinin (HA), a key influenza surface protein for the induction of protective neutralizing antibodies. Particle scaffolds studies include lipid-based NPs (e.g., liposomes or virosomes),[2,3] protein self-assembled NPs (e.g., ferritin NPs),[4,5] polymeric NPs (e.g., poly (lactic-co-glycolic acid) or polystyrene NPs),[6,7] or inorganic NPs (e.g., gold NPs).[8,9] These NP vaccines typically elicit greater immune responses than free subunit antigens due to their enhanced deposition within the lymph nodes (LNs),[10] increased association with antigen presenting cells (APCs),[11–13] and improved activation of B cells via B cell receptor (BCR) cross-linking.[14,15]

NP size is critical for augmenting immune responses through enhanced trafficking to and accumulation in LNs,[10,11] thereby increasing LN-resident APC interaction and B cell activation.[16,17] For instance, polystyrene and virus-like particles of 20–200 nm in diameter effectively drain from injection sites into lymphatic vessels for enhanced trafficking to draining LNs.[10] Gold NPs of 50–100 nm show increased deposition and retention in LNs as compared to smaller counterparts

M. N. Vu, H. G. Kelly, Dr. H.-X. Tan, R. Esterbauer, Prof. T. P. Davis, Dr. N. P. Truong, Dr. A. K. Wheatley, Prof. S. J. Kent
Australian Research Council Centre of Excellence in Convergent Bio-Nano Science and Technology
Monash University
Parkville, VIC 3052, Australia
E-mail: nghia.truong@monash.edu; a.wheatley@unimelb.edu.au; skent@unimelb.edu.au

M. N. Vu, Prof. T. P. Davis, Dr. N. P. Truong
Monash Institute of Pharmaceutical Sciences
Monash University
Parkville, VIC 3052, Australia

The ORCID identification number(s) for the author(s) of this article can be found under https://doi.org/10.1002/adhm.202002142

DOI: 10.1002/adhm.202002142

M. N. Vu, H. G. Kelly, Dr. H.-X. Tan, Dr. J. A. Juno, R. Esterbauer, Dr. A. K. Wheatley, Prof. S. J. Kent
Peter Doherty Institute for Infection and Immunity
University of Melbourne
Melbourne, VIC 3000, Australia

M. N. Vu
Department of Pharmaceutics
Hanoi University of Pharmacy
Hanoi 10000, Vietnam

Prof. T. P. Davis
Australia Institute of Bioengineering & Nanotechnology
University of Queensland
Brisbane, QLD 4072, Australia

Prof. S. J. Kent
Melbourne Sexual Health Centre and Department of Infectious Diseases, Alfred Hospital and Central Clinical School
Monash University
Melbourne, VIC 3004, Australia

(5–15 nm).[11] Similarly, ferritin NPs (≈40 nm) rapidly settle in follicular dendritic cell (FDC) rich areas within germinal centers (GCs) in draining LNs, where high affinity antibody-producing B cells are selected.[16] Further, HIV Env trimers decorated onto the surface of liposomes (≈150 nm) elicit greater induction of GC B cells and follicular helper T (Tfh) cells as compared to free antigens.[17] Despite the advantages of increasing LN trafficking and retention, optimal design principles (e.g., type of NPs, strategy of loading antigens, manufacturing technology, etc.) and the immune mechanisms within the draining LNs that underpin improved immunity of NP-based vaccines remain unclear.

Liposomes are a widely implemented NP platform for both drug and vaccine delivery, with a well-established clinical record of safety and efficacy.[18] For example, Inflexal V, a licensed virosome-based vaccine with a diameter of ≈150 nm, has shown an excellent immunogenicity and tolerability profile in both healthy and immunocompromised people.[3] However, this vaccine was discontinued in 2014 due to bacterial contamination during a complicated and multi-step manufacturing process. Simplifying the production procedure of liposome vaccines is critical to effectively harness this promising platform.[19,20] Traditional methods for production of liposome vaccine can also suffer from poor batch-to-batch reproductivity, difficulty in scale up, and a risk of temperature control driven lipid and antigen degradation.[21] To overcome these limitations, an alternative approach based on advanced microfluidic technology (NanoAssemblr) has been developed as a simple, robust, scalable, and reproducible method to produce homogeneous liposomes.[20,22] Co-injecting a lipid mixture and an aqueous solution at adjustable flow rates into the microfluidic device rapidly forms liposomes.[20,22]

Another challenge in production of liposome vaccines is the loading of hydrophilic antigens. Hydrophilic antigens can be carried by liposomes via encapsulation inside the liposome core or absorption onto their surface. Barnier–Quer et al. reported that surface-absorbed influenza HA onto liposomes were more immunogenic than encapsulated HA.[2] However, this approach is not ideal as the random orientation of HA absorbed on liposome surface may sterically occlude key antigenic sites, resulting in reduced protective immunity. In addition, absorbed HA is easily detached from the liposome surface, leading to reduced and inconsistent immunogenicity. On the other hand, covalent conjugations of antigen proteins to NPs might disrupt protein structures, altering antibody responses to the antigens.[23] Therefore, it is critical for antigens to be strongly attached in their native conformation onto NP surfaces in order to maximize immunogenicity.

In the present study, noncovalent metal chelation via nitrilotriacetic acid (NTA) was utilized as non-destructive method to attach histidine (his)-tagged antigens onto liposomal surfaces.[23,24] We developed a simple, facile, reproducible, and scalable method to prepare liposomal vaccines targeting the HA protein of influenza. NanoAssemblr technology was used to prepare liposomes containing cobalt-bearing lipids, with polyhistadine-tagged HA immunogens functionalized onto liposome surface via chelating with cobalt ions. Liposomal-attached HA was confirmed to physiologically resemble native HA spikes and elicited both high serum antibody responses and robust protective immunity in mice. Upon administration, increased LN accumulation and deposition of HA-liposomes were observed compared with soluble HA vaccines, driving enhanced induction and expansion of HA-specific B and T cell immunity in the draining LNs. Rapid production and greater mechanistic understanding of how liposomal vaccines drive improved immunogenicity will facilitate rational design of the next influenza vaccine generation.

2. Results

2.1. Preparation of HA-Functionalized Liposomes

To mimic the structure of influenza virus, trimeric HA proteins were attached on the surface of liposomes in their native orientation via chelation between polyhistadine-tagged HA and liposomes bearing cobalt ions (Co). The HA gene consisting of ectodomain of HA from A/Puerto Rico/8/1934 (PR8) influenza strain was C-terminally fused to a hexa-histidine tag, and expressed in Expi293F cells as described previously.[25] Liposomes incorporating with an optimal 2% Co-NTA lipids[24] were prepared using a microfluidic device of the NanoAssemblr bench-top instrument.[20,22] Phosphate buffer saline (PBS) and a lipid mixture of 1,2-distearoyl-sn-glycero-3-phosphocholine (DSPC), cholesterol, and 1,2-dioleoyl-sn-glycero-3-[(N-(5-amino-1-carboxypentyl)iminodiacetic acid)succinyl] cobalt salt (DGS-NTA(Co)) (at a 60:38:2 molar ratio) were injected into two inlets of the microfluidic cartridge to produce liposomes (**Figure 1**a, left). After purification, Co-bearing liposomes were incubated with his-tagged HA for 2 h at room temperature (RT) to form chelate bonds between Co^{2+} and histidine residues, allowing HA-liposome attachment (Figure 1a, right). This simple, scalable, two-step procedure facilitates robust production of HA-liposome vaccine with minimum risk of contamination. To elucidate the exclusive effect of HA attached on the surface of liposomes, unbound proteins were removed via size exclusion chromatography (SEC). Only a small fraction of free HA was observed in the SEC trace (Figure S1, Supporting Information), indicating that a high coupling efficiency between his-tagged HA and Co-bearing liposomes was achieved.[17] Cryogenic transmission electron microscopy (Cryo-TEM) of both plain and HA-liposomes showed a similar intact spherical morphology with a lipid bilayer (Figure 1b). Liposome diameter was also determined using dynamic light scattering (DLS) and shown a small increase from ≈130 to ≈145 nm after attachment with HA, which remained stable after 7 days in PBS at 4 and 37 °C (Figure S2, Supporting Information). Narrow size distributions and relatively similar zeta potentials were observed for both plain and HA-liposomes (Figure 1c,d). These data confirmed the successful synthesis of novel HA-liposomes via a simple and scalable approach.

To verify the attachment and antigenicity of HA on the liposome surface, a capture ELISA was used to assess their reactivity to PR8 HA-specific antibodies. Briefly, soluble HA and liposomes were captured by anti-HA stem antibody (CR9114)[26] coated onto MaxiSorp plates, and their binding to monoclonal antibody 441D6 (HA head domain specific)[27] was calculated (Figure 1e, left). Plain liposomes showed no binding with the antibodies while stem-captured HA-liposomes bound to anti-head antibody with relatively similar affinities to soluble HA (Figure 1e, right). The results confirmed the presence and antigenicity of intact HA proteins anchored onto the liposome surface and suggest the intact HA are appropriately orientated on the liposome.

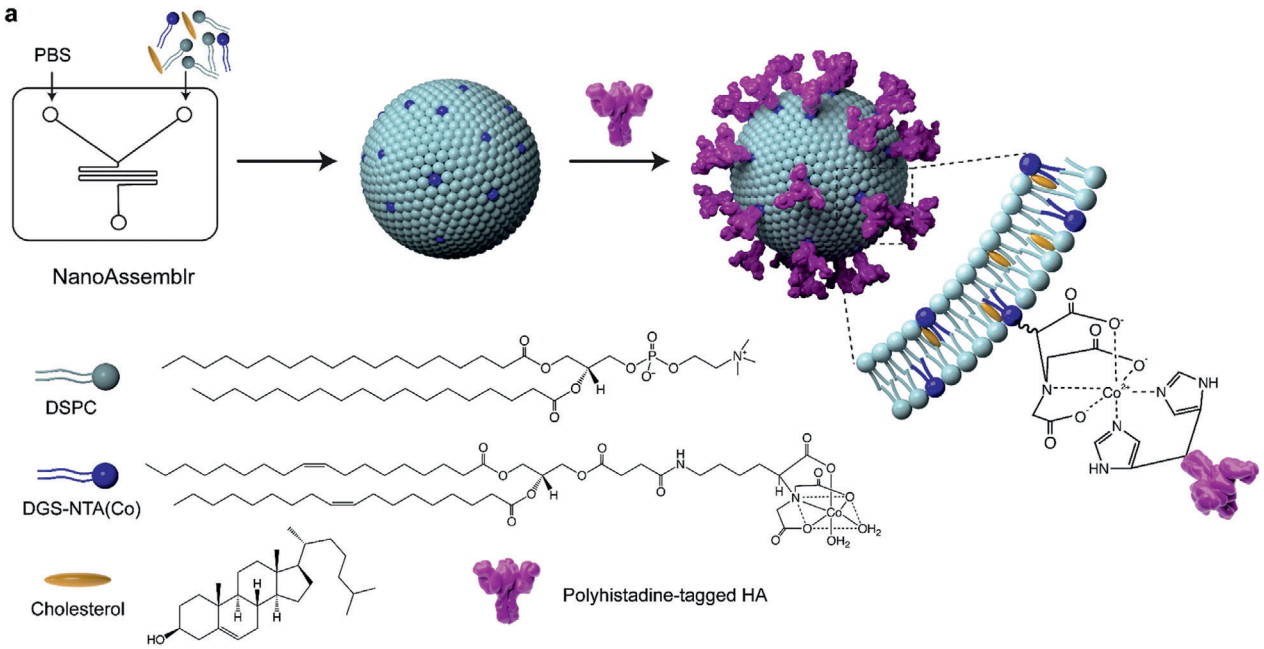

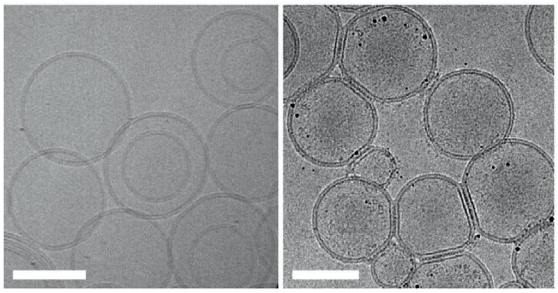

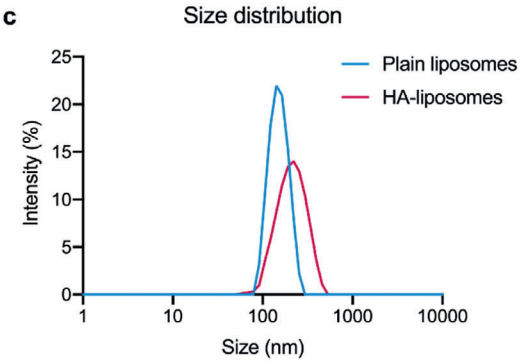

d

Liposome types	Cryo-TEM†	DLS‡		
	d (nm)	d (nm)	PdI	ζ (mV)
Plain liposomes	127.1 ± 25.4	130.2 ± 6.5	0.066	- 7.1 ± 0.5
HA-liposomes	143.8 ± 32.3	145.1 ± 3.8	0.117	- 8.2 ± 1.3

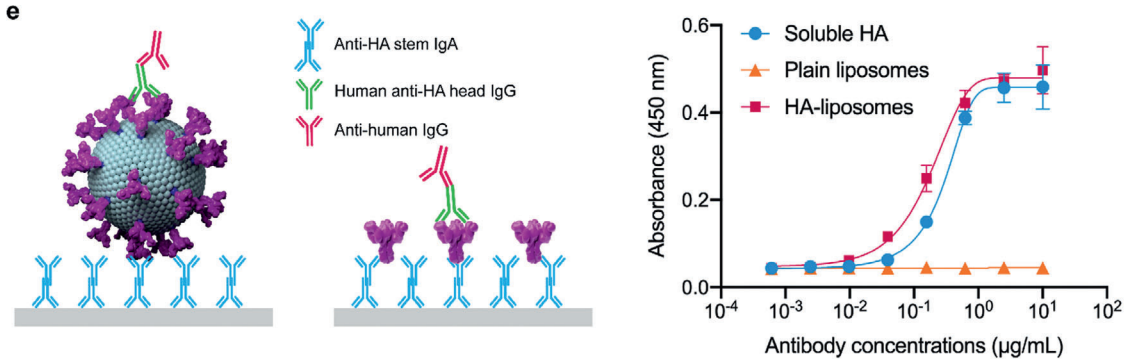

2.2. Immunogenicity and Protective Immunity of HA-Liposomal Vaccines in Mice

We next compared the immunogenicity of HA-liposomes versus soluble HA proteins in mice. C57BL/6 mice (five mice per group) were immunized with a high dose (3.8 μg) or a low dose (0.38 μg) of HA-liposomes or soluble HA (alone or mixed with cobalt-free liposomes). The amount of cobalt in the high dose formulation was ≈0.1 μg, which was reported to be safe for both animal and human use.[28,29] Cobalt-bearing HA-free liposomes were used as negative control and Addavax (a squalene-based oil in water adjuvant) at 50% of total volume was added to all groups 30 min before vaccination (**Figure 2**a). NP size and polydispersity index of the HA-liposomes and Addavax mixture remained constant after 30 min, indicating no negative impacts of Addavax on HA-liposomes (Figure S3, Supporting Information).[30] HA-liposomes elicited significantly higher HA-specific serum IgG titers than a mixture of Co-free liposomes and soluble proteins at both high (≈5.3-fold, $p < 0.05$) and low (≈13.2-fold, $p < 0.001$) HA doses (Figure 2b). Furthermore, the presence of Co-free liposomes in mixture with soluble HA did not show increase HA-specific serum antibody titers when compared to soluble HA alone, indicating minimal adjuvant effects of liposomes alone (Figure 2b). In short, the data shows that display of HA on liposomes but not liposome itself improves the immunogenicity influenza HA in mice.

The protective capacity of HA-liposomes and soluble HA protein was assessed by a virus challenge study. A highly pathogenic dose (2000 $TCID_{50}$ = ≈80LD_{50}) of A/PR/8/1934(H1N1) influenza was used to infect mice intranasally 28 days after immunization. This robust influenza challenge model reliably leads to rapid weight loss of infected mice in the absence of immunity.[16] All ten mice administered with either the liposome control or a low dose of soluble HA (0.38 μg) were euthanized 5 or 6 days post infection respectively after losing more than 20% of their original weight. HA-liposomes (at a low dose) protected two of five immunized mice from the virus challenge. Four out of five mice vaccinated with a high dose (3.8 μg) of soluble antigens survived while all five mice immunized with HA-liposomes (at high dose) survived from the virus infection and showed less weight loss than the ones vaccinated with soluble HA (Figure 2c and Figure S4, Supporting Information). Overall, vaccination with HA-liposomes demonstrated improved protection from highly pathogenic influenza challenge when compared to the soluble antigens.

2.3. HA-Liposomes Increase Antigen Deposition in LN-Resident FDCs and GCs

GCs are formed in secondary lymphoid organs (i.e., in the draining LN following intramuscular vaccination) following antigen exposure by infection or immunization. Within GC, antigen is captured and presented by FDC and B cells undergo antigen-specific proliferation, somatic hypermutation, and affinity maturation. This in turn drives the production of antigen-specific long-lived memory B cells, antibody-secreting plasma cells, and the generation of serum antibodies.[31] Thus, increased deposition and retention of antigens within GC areas would facilitate induction of antigen-specific antibodies and improve protective capacity of administrated vaccines. To assess this hypothesis, here we examined the accumulation and distribution of HA within draining LNs, with the focus on GC areas after HA-liposome as compared to soluble HA administration. We immunized mice intramuscularly with Alexa Fluor 647 (AF647)-conjugated HA either mixed with or attached to Rhodamine B-labeled liposomes and performed histological analyses of the draining inguinal LNs 1, 24, 72 h, 1, and 2 weeks later. Successful labeling liposomes and HA with fluorescent dyes were confirmed by fluorescent intensity measurement (Figure S5 a,b, Supporting Information). GCs were only formed at 7 days following immunization although both liposomes and soluble HA approached the LNs after 1 h injection. They are primarily located in subcapsular sinus (SCS) and colocalized with $CD169^+$ macrophages (Figure S6 a, Supporting Information). From 24 h to 72 h post vaccination, liposomes were found to penetrate into the LNs, and concentrate in $CD35^+$ FDC areas, leading to an increased deposition of HA antigens in FDC network following HA-liposome immunization, which was not observed after soluble HA vaccination (Figure S6 b,c,e, Supporting Information).

At days 7 and 14 post-immunization, $GL7^+$ GCs were formed. While HA-liposomes were observed to localize within follicular regions in close proximity to $CD35^+$ FDC and $GL7^+$ GC areas, soluble HA and liposome control were primarily distributed in the SCS (**Figure 3**a–c and Figures S6d and S7, Supporting Information). When quantitated by colocalization analysis, at day 14, 33.8 ± 6.9% and 17.3 ± 5.7% of HA were shown to concentrate within GC and FDC areas respectively following HA-liposome immunization, which was significantly higher than the percentage of soluble HA localized in these regions (with 18.1 ± 3.1% in GCs and 8.0 ± 2.0% in FDCs, $p < 0.01$) (Figure 3d, left and middle). In addition, the proportion of HA colocalized with liposomes after HA-liposome vaccination (75.3 ± 8.8%) was significantly higher than observed in mice immunized with soluble HA mixed with Co-free liposomes (46.4 ± 6.6%, $p < 0.001$, Figure 3d, right). This indicated association between his-tagged HA and Co-bearing liposomes was stable in vivo for over 2 weeks and suggests that liposomal formulation is critical for enhanced HA accumulation within LNs. Increased formation of GCs and FDCs following HA-liposome administration was also observed compared to soluble HA immunizations (Figure 3a) with the surface area of GC and FDC regions after HA-liposome immunization significantly

Figure 1. Liposome preparation and characterization. a) Schematic illustration of preparation of plain liposomes which contain DGS-NTA(Co), DSPC, and cholesterol using NanoAssemblr microfluidic device and bindings of these liposomes with his-tagged PR8 HA to form HA-attached liposomes. b) Cryo-TEM images of plain liposomes (left) and HA-liposomes (right), scale bars = 100 nm. c) Size distribution of plain and HA-attached liposomes measured by DLS. d) Physicochemical properties of plain and HA-attached liposomes measured by cryo-TEM and DLS. †Diameters of the liposomes measured by cryo-TEM were calculated by FIJI. ‡DLS analysis was performed at 25 °C with reported values averaged over three measurements. e) Antigenicity of HA spikes in soluble forms and attached on the surface of liposomes. Schematic illustration of capture ELISA to assess the antigenicity of soluble HA and HA-liposomes (left). Reactivity of soluble HA, HA-liposomes, and plain liposome control with anti-HA head antibodies (right).

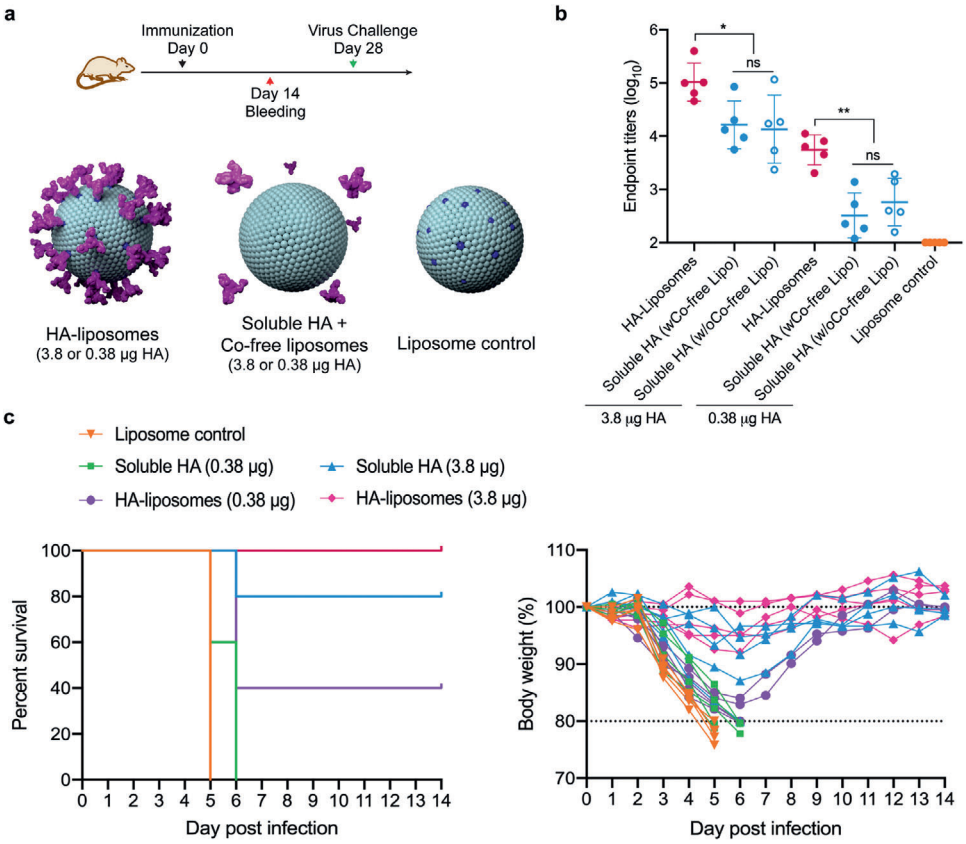

Figure 2. Immune responses and protective immunity induced in mice immunized with soluble HA and HA-liposomes. Seven groups of C57BL/6 mice ($n = 5$) were immunized with either HA-liposomes or soluble HA (with or without presence of Co-free liposomes) at a low dose (0.38 μg) or a high dose (3.8 μg) of HA proteins, plain liposomes were used for control group. a) Schematic illustration of experimental design. b) HA-specific IgG titers measured in mouse sera at day 14 post vaccination using a direct ELISA. Data are presented as mean ± SD and representative of one of two independent experiments. Statistical significance was determined by a paired two-tailed *t*-test; ns $p > 0.05$, * $p < 0.05$, ** $p < 0.01$. c) Five groups of C57BL/6 mice ($n = 5$) were immunized with liposome control, HA-liposomes, or soluble HA mixed with Co-free liposomes at a low dose (0.38 μg) or a high dose (3.8 μg) of HA proteins. Protection of immunized mice from A/PR8/34 virus challenge at a viral dose of 2000 $TCID_{50}$ on day 28 post immunization. Survival rates (left) and changes in body weight (right) of mice in 14 days after virus challenge were monitored. Data are presented as representative of one of two independent experiments.

increased ≈3.5-fold, ($p < 0.0001$) and ≈3.7-fold ($p < 0.001$) respectively compared to animals vaccinated with free HA (Figure 3e).

2.4. HA-Liposomes Enhance Antigen-Specific GC Responses

HA-liposomes drove increased formation of GC areas in draining LNs and augmented antigen deposition within these areas as compared to soluble HA. We next examined the extent to which HA-liposomes drive enhanced GC formation and antigen-specific B cell responses. Mice were immunized as before and single cell suspensions from draining inguinal and iliac LNs recovered at days 14 post-immunization. The magnitude and specificity of the GC responses were examined by flow cytometry and fluorescently labeled HA B cell probes[25] (Gating of GC B cells ($IgD^{-}B220^{+}GL7^{+}CD38^{lo}$) is shown in Figure S8 a, Supporting Information). Enhanced GC formation was observed after HA-liposome vaccination (29.6 ± 3.0%) (**Figure 4**a) as compared to immunization with soluble HA (19.6 ± 4.2%, $p < 0.01$) and liposome controls (8.1 ± 3.5%, $p < 0.0001$). Further, we observed a significantly higher proportion of HA-specific GC B cells in HA-liposome vaccinated mice (17.7 ± 3.5%) in comparison with animals immunized with soluble HA (10.2 ± 2.9%, $p < 0.01$) (Figure 4b).

We next quantified HA-specific memory B cells ($IgD^{-}B220^{+}CD38^{+}GL7^{lo}$) in draining inguinal and iliac LNs. Populations of HA-specific memory B cells were readily observed in mice immunized with HA-liposomes compared to controls (Figure S8 b, Supporting Information). However, all mice groups were at relatively low frequencies (with less than 1% of total memory B cells) in line with the relatively early time point after immunization (day 14). The presence of Co-free liposomes in the mixture with soluble HA did not show significant difference in frequencies of both HA-specific GC and memory B cells (Figure S8 c, Supporting Information). Overall, our data confirmed that HA-liposomes drive enhanced antigen-specific GC B cells, but not memory B cell responses to vaccination.

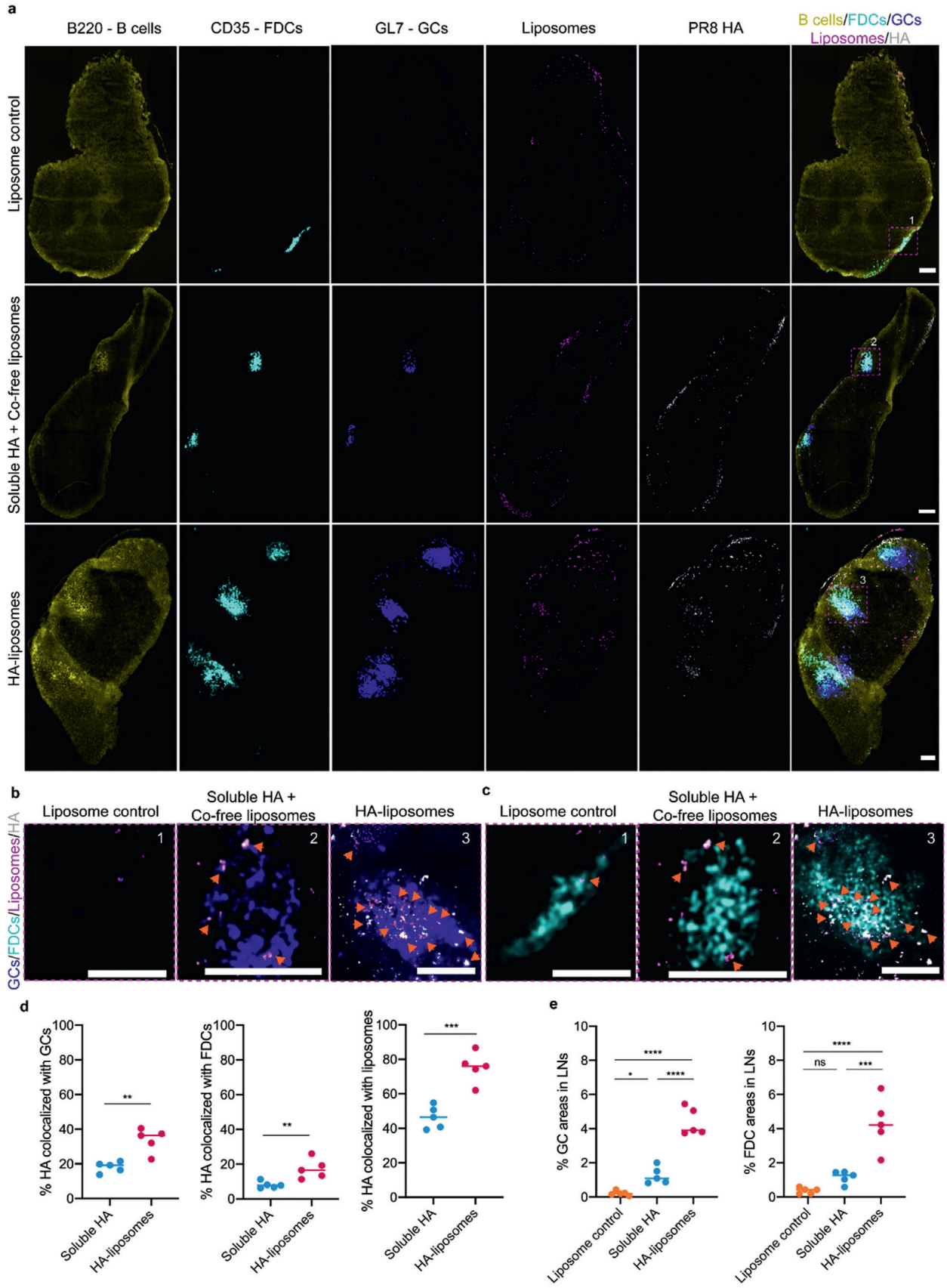

2.5. HA-Liposomes Elicit Improved Follicular Helper T Cell Responses

Follicular helper T (Tfh) cells support antigen-specific B cell differentiation and GC formation within LNs, and therefore are critical to the generation of effective antibody responses to vaccination.[31,32] In contrast, T follicular regulatory (Tfr) cells are another specialized subset of $CD4^+$ T cells present in LNs, which derive from $Foxp3^+$ regulatory (Treg) cells and can act as suppressors of GC responses.[33] Little is known about Tfh and Tfr responses to liposome-based vaccines. We hypothesized that the augmented induction of HA-specific GC B cells observed after HA-liposome immunization might be impacted by the relative formation of Tfh or Tfr cells. Single cell suspensions from draining inguinal and iliac LNs were stained 14 days after vaccination and analyzed by flow cytometry. As Tfh cells are relatively poor producers of cytokines, it is challenging to assess traditional intracellular cytokine staining, thus in this study, a more reliable and sensitive surface activation-induced marker assay was used.[34] The gating strategy to identify total Tfh cells ($CD4^+CXCR5^{hi}Bcl\text{-}6^{hi}PD\text{-}1^{hi}$) as well as $Foxp3^-$ Tfh and $Foxp3^+$ Tfr cells are shown in Figure S9 a, Supporting Information. Increased Tfh responses were observed in the LNs of mice after vaccination with HA-liposomes compared to soluble HA (mean 1.1% versus 0.5%, $p < 0.01$) (**Figure 5**a). Further, we observed a significant increase of ≈2.3-fold in the percentage of $Foxp3^-$ Tfh cells in mice immunized with HA-liposomes as compared to those vaccinated with soluble antigens ($p < 0.001$; Figure 5b, left). However, frequencies of $Foxp3^+$ Tfr cells were also significantly higher (≈1.8-fold, $p < 0.01$) following HA-liposome immunization than soluble HA vaccination (Figure 5b, middle). Therefore, the ratio of Tfh to Tfr cells was increased in HA-liposome vaccinated mice compared to soluble HA vaccinated mice, although the difference was not significant (Figure 5b, right). Co-free liposomes administered with soluble HA did not show marked induction of Tfh and Tfr cells (Figure S9 b,c, Supporting Information). Overall, HA-liposome immunization increases LN Tfh frequencies, facilitating improved serological responses, but without altering the ratio of Tfh to Tfr cells.

3. Discussion

This study utilized advanced NanoAssemblr technology to prepare cobalt-bearing liposomes to overcome the limitations of conventional liposome production methods.[22] By injecting the lipid mixture and aqueous solution, homogeneous liposomes containing cobalt-bearing lipids were rapidly formed. The metal chelation strategy was then used to attach liposomes with C-terminally his-tagged HA proteins, which offers a number of advantages. First, compared to covalent linkage, noncovalent chelate coupling has a higher efficiency.[35] This coupling strategy results in ≈240 HA proteins attached to each liposome,[36] which was much higher than some other methods, such as the only 8 spikes on ferritin NPs.[4] Increased local concentrations of antigens on liposome surface might further improve immune responses.[4,24,37] Exploiting the similar chelating strategy, cobalt porphyrin-phospholipid (CoPoP) was also used to attach his-tagged proteins onto liposomes, however, the hindrance of cobalt ions at lipid tails in lipid biolayers required histidine penetration into liposome membrane and thus decreased coupling efficiency.[38] Second, trimers were attached via hexahistidine residues in the C-terminal domain, resulting in naturally oriented attachment of HA proteins onto liposomes. Our antigenicity data confirmed similar binding affinities between HA spikes anchored onto liposomes and soluble proteins with PR8 HA-specific antibodies, suggesting efficient exposure of HA epitopes when presented upon the liposomes. Third, cobalt ions can form highly stable linkage with HA in vivo,[35] leading to more than 75% HA colocalized with liposomes within LNs even 2 weeks after immunization. The high stability of antigen-liposome anchoring is critical to augmented GC and output antibody responses.[17] Last but not least, this formulation method only requires mixing and incubating at room temperature, which is simple, scalable, and easily translatable to resource poor settings where cold-chain dependent vaccines can be problematic.

HA-liposomes elicited significantly higher serum antibody titers and as a result, greater protection in vaccinated mice from highly pathogenic viral infection as compared to soluble HA. Similarly, immunization with antigen-attached NPs triggered augmented GC induction and thus induced increased antibody responses in mice and non-human primates (NHPs).[17,24,39,40] Two mechanisms could contribute to this enhanced GC formation: (i) increased NP trafficking and retention within LNs and (ii) decoration of multiple antigen copies onto NP surface could significantly augment antigen-specific B cell activation.[41] Vaccine NPs can improve transport to and retention within draining LNs in size and complement-dependent manner.[41] A study on gold NPs reported that small particles (<15 nm) rapidly entered the LN follicles, but then quickly cleared within 48 h after injection while larger NPs (50, 100 nm) were found in follicles within 12 h and retained there for several weeks post immunization.[11] Similarly, in the present study, 145-nm HA-liposomes rapidly approached the LNs within 1 h, enriched in FDC areas of B cell follicles within 24 h and maintained there for at least 2 weeks post vaccination.

Figure 3. Deposition of HA-liposomes on follicular dendritic cells (FDCs) and within germinal centers (GCs). a) Three groups of C57BL/6 mice ($n = 5$) were immunized with either HA-liposomes, mixture of soluble HA, and cobalt-free liposomes at a high dose (3.8 μg) of HA proteins, or plain liposome control. Liposomes were modified to incorporate 16:0 Liss Rhod PE (magenta) and PR8 HA were labeled with AF647 (gray). At day 14 post immunization, draining inguinal lymph nodes were harvested, sectioned and stained with B220 BV510 (B cells–yellow), CD35 BV421 (FDCs–cyan), and GL7 AF488 (GCs–blue). b,c) Inset images of follicle regions were magnified to allow visualization of HA and liposomes colocalized with either (b) GC or (c) FDC areas. Images were captured by a Zeiss LSM780 inverted confocal microscopy. Scale bars = 150 μm. d) Percentage of HA colocalized with GCs (left), FDCs (middle), and liposomes (right) analyzed using colocalization tool in FIJI. Data are presented as mean ± SD, $n = 5$ images from five different lymph nodes of five mice. Statistical significance between soluble HA and HA-liposome groups was determined by a paired two-tailed *t*-test; ** $p < 0.01$, *** $p < 0.001$. e) Percentage of GC (left) and FDC (right) areas in total area of lymph node, measured as pixels above background using FIJI. One-way ANOVA with Tukey's pairwise comparisons post-hoc test was used to assess statistical significance between three group data; ns $p > 0.05$, * $p < 0.05$, *** $p < 0.001$, **** $p < 0.0001$.

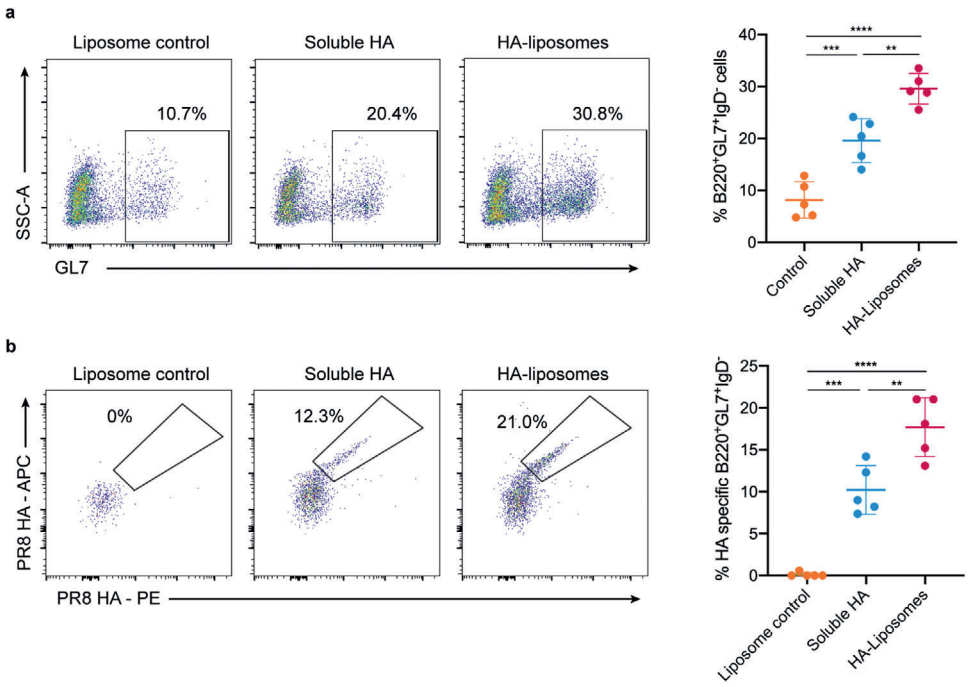

Figure 4. Germinal center responses in lymph nodes of mice immunized with soluble HA and HA-liposomes. Three groups of C57BL/6 mice ($n = 5$) were immunized with either HA-liposomes, mixture of soluble HA, and cobalt-free liposomes at a high dose (3.8 μg) of HA proteins, or plain liposome control. At day 14 post immunization, both draining inguinal and iliac lymph nodes were harvested, single cells were isolated, pooled, and stained with antibodies specific for germinal center B cells. a) Representative flow plot (left) of GC B cell populations ($IgD^{-}B220^{+}GL7^{+}CD38^{lo}$) and frequencies of GC B cells in total $B220^{+}IgD^{-}$ B cells (right). b) Representative flow plot of PR8 HA-specific GC B cells (left) and proportion of HA-specific GC B cells in total GC B cells (right). Data are presented as mean ± SD and representative of one of two independent experiments. Each dot in plots represents one animal. One-way ANOVA with Tukey's pairwise comparisons post-hoc test was used to assess statistical significance between three group data; ** $p < 0.01$, *** $p < 0.001$, **** $p < 0.0001$.

Depot effects of liposomes at injection sites could also contribute to continuous delivery of antigens to the LNs.[18] The long-term persistence of antigens within LNs might be crucial for maintenance of immunological memory.[42,43] In addition, complement opsonization onto NP surface and their consequent activation of pattern recognition receptors (PRRs) on immune cells often play a role on NP deposition within LNs.[1,41] For example, both HIV Env and HA-ferritin NPs (≈40 nm) were found to show greater accumulation into GC and FDC areas of draining LNs mediated by mannose binding lectin (MBL) recognition of sugars on the NP surface via lectin complement pathway.[16,44] In line with other reports,[45] we find HA-liposomes (≈145 nm) could enhance FDC and GC formation, with improved antigen retention although any the contribution of complement or PRR pathways remains unclear (**Figure 6**).

In addition, compared to soluble antigens, introduction of multiple antigen copies presented onto NP surface to B cells can enhance antigen-specific B cell activation.[41] While soluble antigens only engage with a single BCR, dense array of antigens allows both bivalent recognition by individual BCR and cross-linking of multiple BCRs on a single cell, which in turn increase antigen binding avidity[46] and promote potent B cell activation.[27,47,48] Furthermore, extent of BCR engagement is dependent on antigen density on NP surface.[24,49,50] In the present study, with ≈240 HA proteins displayed on one liposome, we estimated that the antigen spacing was ≈15 nm apart, which allowed maximal BCR cross-linking, and thus enhanced antigen-specific B cell activation.[1] Although augmented HA-specific GC B cell responses following HA-liposome immunization were demonstrated as a result, direct observation of BCR cross-linking by HA-liposomes has not been achieved, which will be investigated in future studies.

The formation and expansion of GCs are regulated by Tfh cells, positive regulators of the size and quality of GC responses, and Tfr cells which act as suppressors of the GC.[33] The size of antigen-functionalized particles was reported to influence Tfh cell generation.[51] In particular, as compared to small particles (40 nm), larger ones (200 nm) were found to sustain antigen presentation by DCs and maintain DC-T cell interactions into stage 3 (>72 h) of activation, which drove enhanced Tfh differentiation and in turn supported GC reactivities.[51] This is consistent with other studies reporting that only large particles (e.g., 150, 180-nm liposomes[17,45] or 130-nm polymeric particles[52]), but not smaller particles (e.g., 25-nm virus-like particles[53] and 40-nm protein-based particles[44]) improved Tfh cell frequencies relative to free antigens. Here, we also found increases in Tfh cell proportions in LNs of mice vaccinated with HA-liposomes particles (≈145 nm) compared to free HA, confirming a critical role of particle-presented antigen on Tfh cell responses. However, effects of antigen-decorated particles and their size on Tfr cell reactions and Tfh/Tfr ratio remain under-explored and require further investigation.

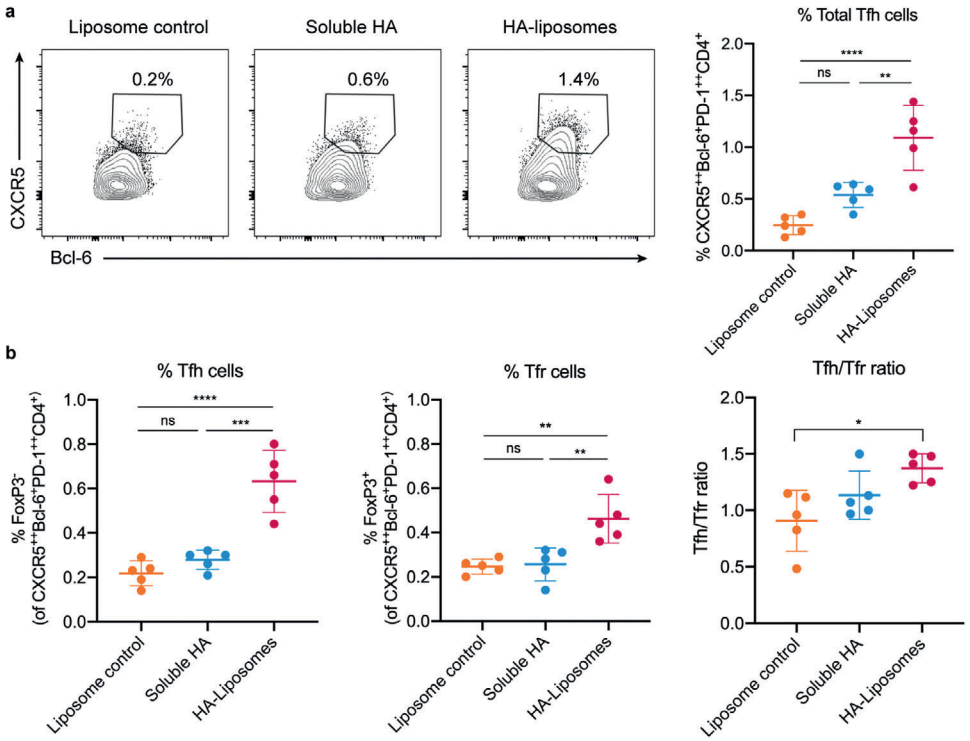

Figure 5. Ex vivo follicular helper T (Tfh) cell responses in lymph nodes of mice immunized with soluble HA and HA-liposomes. Three groups of C57BL/6 mice ($n = 5$) were immunized with either HA-liposomes, mixture of soluble HA, and cobalt-free liposomes at a high dose (3.8 μg) of HA proteins, or plain liposome control. At day 14 post immunization, both draining inguinal and iliac lymph nodes were harvested, single cells were isolated and stained with antibodies specific for Tfh cells. a) Representative flow plot (left) of total Tfh cell populations ($CD4^+CXCR5^{hi}Bcl\text{-}6^{hi}PD\text{-}1^{hi}$) and frequencies of total Tfh cells in $CD4^+$ T cells (right). b) Frequencies of Tfh cells ($Foxp3^-$, left) and Tfr cells ($Foxp3^+$, middle) in total $CD4^+$ T cells. Ratio of Tfh to Tfr cells in lymph nodes (right). Data are presented as mean ± SD and representative of one of two independent experiments. Each dot in plots represents one animal. One-way ANOVA with Tukey's pairwise comparisons post-hoc test was used to assess statistical significance between three group data; ns $p > 0.05$, * $p < 0.05$, ** $p < 0.01$, *** $p < 0.001$, **** $p < 0.0001$.

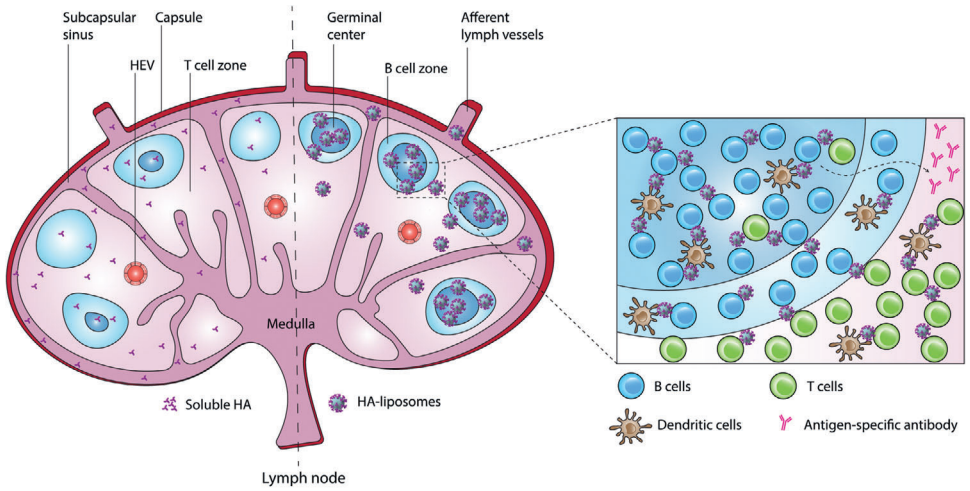

Figure 6. Distribution of antigen within lymph nodes following soluble HA and HA-liposome immunization. Compared to soluble HA (left), HA-liposome administration (right) enables increased retention of antigens in B cell follicles with assistance of follicular dendritic cells and helper T cells, leading to augmented induction of antigen-specific germinal center B cells and in turn improved production of antigen-specific antibodies.

4. Conclusion

In summary, advanced microfluidic technology enables the rapid preparation of liposomal vaccines with attachment of HA antigens onto their surface, driving improved protective immunity in immunized mice. Although the liposome itself showed minimal adjuvant effects, additional adjuvants can be incorporated into the NP in future works to further enhance vaccine efficiency. A greater understanding of the mechanisms that underpin the immunogenicity of NP vaccines will facilitate the rational design next-generation liposomal subunit vaccines with favorable properties for combatting endemic and pandemic virus infections.

5. Experimental Section

Expression of Recombinant HA: Recombinant PR8 HA protein was synthesized as described previously.[25] HA gene (GeneArt) consisting of the ectodomain of HA C-terminally fused to a hexa-histidine tag was cloned into mammalian expression vectors. HA DNA was then transfected into Expi293F cells (Life Technologies) using ExpiFectamine 293 transfection reagents with 1 μg DNA in 2.5×10^6 cells. The his-tagged HA was purified by immobilized metal affinity chromatography using nickel-NTA Agarose (Life Technologies). The eluted protein was concentrated and loaded on a Superose 6 column (GE Healthcare) in PBS. The fraction corresponding to trimeric HA was pooled and concentrated. For imaging studies, HA proteins were then fluorescently labeled with Alexa Flour 647 (AF647) by using AF647 protein labeling kit (Life Technologies).

Synthesis of HA-Functionalized Liposomes: Lipids used for liposome synthesis, including 1,2-distearoyl-sn-glycero-3-phosphocholine (18:0 PC or DSPC), cholesterol, 1,2-dioleoyl-sn-glycero-3-[(N-(5-amino-1-carboxypentyl)iminodiacetic acid)succinyl] cobalt salt (18:1 DGS-NTA(Co)), and 1,2-dipalmitoyl-sn-glycero-3-phosphoethanolamine-N-(lissamine rhodamine B sulfonyl) (ammonium salt) (16:0 Liss Rhod PE) were purchased from Sigma Aldrich. Plain liposomes were synthesized by using a microfluidic mixture (Precision NanoSystems). One volume of lipid mixtures at the appropriate ratios in chloroform:ethanol (1:10 v/v) and three volumes of PBS were injected into the micro-mixer at a total flow rate of 8 mL min^{-1} and a flow rate ratio of 3:1 (2 mL min^{-1} for lipid mixtures and 6 mL min^{-1} for PBS). The liposomes were dialyzed against PBS overnight to remove inorganic solvents, and then concentrated to 10 mg mL^{-1} lipids by ultrafiltration using a 100 kDa Ultracel membrane (Merk Millipore). Next, the liposomes were extruded for a minimum of 20 times through 0.4-, 0.2-, and 0.1-μm filters using a mini-extrusion device (Avanti Polar Lipids) at 60 °C (higher than T_m of the lipids) to form unilamellar liposomes.

Protein attachment to the liposomes was carried out by incubating his-tagged HA and liposomes at a 1:10 mass ratio of proteins:lipids for 2 h at room temperature. The unbound proteins were removed from the liposomes by size exclusion chromatography using a Superose 6 column. The liposome fractions were collected, pooled, and concentrated by ultrafiltration with the 100-kDa Ultracel membrane.

Characterization of HA-Functionalized Liposomes: DLS: Dynamic diameter and zeta potential of plain and HA-attached liposomes (50 μg mL^{-1} in PBS) were measured by DLS using a Malvern Zetasizer Nano Series with a 4 mW He-Ne ion laser ($\lambda = 633$ nm). Data measurement and analysis were performed at an angle of 173° and a temperature of 25 °C. Cryo-TEM: 4 μL of 1 mM liposomes in PBS were put onto copper grids (200-mesh), which coated with holey carbon film (Quantifoil R1.2/1.3) and pre-glow discharged in a Pelco glow discharge unit. To form a thin film on the grids, we blotted samples for 3 s at a blot force of −6 in a Vitrobot plunge freezer system (FEI), and plunged them into liquid ethane at 5 °C. The vitrified samples were transferred to a Gatan 626 cryoholder and then imaged by a Tecnai 12 TEM at a voltage of 120 kV and temperatures at −175 to −170 °C. Images were processed by a Gatan Eagle high-resolution CCD camera (4000 × 4000). Fluorescence Measurement: Fluorescence spectra of fluorescently-labeled and control liposomes were obtained using a fluorescence spectrophotometer (Shimadzu RF-501 PC) at an excitation wavelength of 535 nm for Rhodamine B and 635 nm for AF647, and slit widths of 5 nm for both excitation and emission.

Antigenicity ELISA: Capture ELISA was used to verify antigenicity of soluble HA and HA spikes attached onto liposomes. To start, 96-well MaxiSorp plates (Thermo Fisher Scientific) were coated overnight at 4 °C with 100 μL of anti-HA stem monoclonal antibody CR9114 IgA at 2 μg mL^{-1} in PBS. After blocked with 200 μL of 5% skim milk in PBS for 2 h at RT, the plates were incubated with 100 μL of HA proteins at 5 μg mL^{-1} in either soluble form or attached with liposomes in 2 h at RT. Plain liposomes at equivalent lipid molar were used as control group. Next, the plates were incubated with a fourfold serial dilution of anti-HA head IgG antibodies (441D6) and VRC01 as negative control with a starting concentration of 10 μg mL^{-1} in 2 h at RT. Secondary antibody rabbit anti-human IgG conjugated with horseradish-peroxidase (HRP) (DAKO) at 1:30 000 in 5% skim milk was added to the plates and incubated for 1 h at RT. After each step, the plates were washed twice with PBS containing 0.05% Tween 20, then twice with PBS. The plates were then developed by 80 μL of tetramethylbenzidine (TMB–Sigma Aldrich) for 7 min, and halted by adding 50 μL of 0.16 M sulfuric acid. Absorbance was measured at 450 nm.

Mouse Immunization: C57BL/6 female mice (6 to 8 weeks old, $n = 5$ mice per group) were anesthetized by isoflurane inhalation, and immunized with either HA-liposomes or soluble HA (alone or mixed with cobalt-free liposomes) at a high dose (3.8 μg) or a low dose (0.38 μg) of HA proteins, along with 50% of Addavax (InvivoGen) in a total volume of 100 μL. Plain liposomes formulated with 50% Addavax were used for control mice. All mice were injected intramuscularly with 50 μL of the vaccine solutions in each leg.

Mouse Serum ELISA: HA-specific IgG titers in immunized mice at day 14 post-vaccination were detected by a direct ELISA. Ninety-six-well MaxiSorp plates were coated with 100 μL of 2 μg mL^{-1} PR8 HA overnight at 4 °C before blocked with 200 μL of 5% skim milk in PBS in 2 h at RT. Mouse sera were diluted in the blocking solution, starting at 1:100 with fourfold serial dilutions and added to the plates, then incubated in 2 h at RT. The plates were incubated with secondary antibody (goat anti-mouse IgG-HRP conjugation) at 1:10 000 for 1 h at RT. After each step, the plates were washed twice with 0.05% Tween 20 in PBS, and then twice with PBS. TMB solution (80 μL) was added to the plates for 7 min before plates were halted with 50 μL of 0.16 M sulfuric acid. Absorbance was measured at 450 nm. ELISA endpoint titers were calculated as the reciprocal serum dilution giving signal 3× above background.

Viral Challenging: At day 28 post immunization, mice were anesthetized by isoflurane inhalation prior to infection with 2000 $TCID_{50}$ of A/PR/8/34(H1N1) virus via nasal administration. The mice were monitored for clinical signs and weight loss for 14 days post infection. Mice were killed if 20% of their original weight was lost.

Flow Cytometric Detection of HA-Specific B Cells: Mice were sacrificed at day 14 post immunization and both inguinal and iliac LNs were harvested. Single cells were isolated and stained with Aqua viability dye (Thermo Fisher Scientific) and Fc-blocked with anti-CD16/32 antibody (clone 93, BioLegend). Cells were then labeled with PR8 HA-PE and PR8 HA-APC probes, and the following antibodies: F4/80 BV786 (BM8; BioLegend), B220 BUV737 (RA3-6B2; BD), CD45 Cy7-APC (30-F11; BD), IgD BUV 395 (11-26c.2a; BD), GL7 AF488 (GL7; BioLegend), CD38 Cy7-PE (clone 90; BioLegend). Cells were then washed twice, fixed in 1% formaldehyde solution, and analyzed on a BD LSR Fortessa using BD FACSDiva. Flow cytometry data were processed using FlowJo v10.

Flow Cytometric Detection of Ex Vivo Follicular Helper T Cells: Inguinal and iliac LNs were harvested at 14-day post immunization as described above. Single cell suspensions were first labeled with Live/Dead Red (Life Technologies) and then surface stained with CD3 BV510 (145-2C11; BioLegend), PD-1 BV786 (29F.1A12; BioLegend), CXCR5 BV421 (L138D7; BioLegend), CD4 BUV737 (RM4-5; BD), B220 BV605 (RA3-6B2; BD), F4/80 PE-Dazzle 594 (T45-2342; BD). Cells were washed, fixed, and permeabilized by using Fixation/Permeabilization Solution Kit (BD) before intercellularly labeled with Bcl-6 AF647 (IG191E/A8; BioLegend) and Foxp3 PE (MF-14; BioLegend). Cells were washed twice, fixed with 1% formaldehyde, and

acquired on a BD LSR Fortessa using BD FACSDiva. Flow cytometry data were analyzed using FlowJo v10.

Confocal Microscopy: For imaging studies, liposome composition was modified to incorporate 2% of 16:0 Liss Rhod PE while HA proteins were labeled with AF647 by using AF647 Protein Labeling Kit (Life Technologies). C57BL/6 female mice (6 to 8 weeks old, $n = 5$ mice per group) were immunized with either fluorescently-labeled liposome control, soluble HA physically mixed with cobalt-free liposomes, or HA-liposomes as previously described. Inguinal LNs of the immunized mice were collected into OCT Embedding Compound (Tissue-Tek) at 1, 24, 72 h, 7, and 14 days post vaccination, snap-frozen, and stored at −80 °C overnight. Tissues were then sectioned into 7-µm slices (Leica) and dried overnight at RT. The tissues were fixed with cold acetone (4 °C) in 10 min, rehydrated in PBS in another 10 min at RT, and blocked with 5% bovine serum albumin (BSA–Millipore Sigma), 2% normal goat serum, and 1:50 rat anti-mouse CD16/CD32 Fc block. Cells were then stained with CD169 BV605 (3D6.122, BioLegend), CD35 BV421 (8C12; BD), B220 BV510 (RA3-6B2, BD), and GL7 AF488 (GL7; BioLegend). Slides were washed, mounted with Prolong Diamond Antifade Mountant (Life Technologies), and imaged by Zeiss LSM780 inverted confocal microscopy using Zen Black software. Images were captured with a 20× 0.8NA air objective at 1 airy unit and 512 × 512 pixel resolution with a pixel dwell time of 10 µs pixel^{-1}. Images were then processed using FIJI software. Percentage area of GCs and FDCs was calculated by measuring GL7 and CD35 pixels relative to the total area of LNs respectively. Colocalization analysis was performed using Coloc 2 plugin in FIJI, Mander split coefficients were reported as levels of colocalization between channels.

Statistical Analysis: Data were presented as mean ± S.D ($n = 5$). Statistical analyses were performed using GraphPad Prism version 8. For serum antibody study, a paired two-tailed *t*-test was performed. For all other analyses comparing multiple groups, one-way ANOVA with Tukey's pairwise comparisons post-hoc test was used. *P* value of less than 0.05 ($p < 0.05$) was considered to be significant for all statistical tests.

Study Approval: Mouse studies were approved by the University of Melbourne Animal Ethics Committee (Ethic number 1714193).

Supporting Information

Supporting Information is available from the Wiley Online Library or from the author.

Acknowledgements

The authors would like to thank Dr. Andrew Leis (University of Melbourne) for assistance with Cryo-TEM and Mr. Nam Dao (Monash University) for his help on liposome preparation. T.P.D., N.P.T., and S.J.K. acknowledge the receipt of a Discovery Project grant (DP200100231) from the Australian Research Council (ARC). N.P.T. is grateful for the award of a DECRA Fellowship from the ARC (DE180100076). This work was carried out within the Australian Research Council (ARC) Centre of Excellence in Convergent Bio-Nano Science and Technology (Project No. CE140100036). M.N.V. acknowledges the financial support from Monash Graduate Scholarship (MGS) and Monash International Postgraduate Research Scholarship (MIPRS).

Conflict of Interest

The authors declare no conflict of interest.

Data Availability Statement

The data that support the findings of this study are available from the corresponding author upon reasonable request.

Keywords

follicular helper T cells, germinal centers, influenza vaccines, liposomes, microfluidic mixers, nanoparticle-based vaccines

Received: January 25, 2021
Revised: February 15, 2021
Published online: March 9, 2021

[1] H. G. Kelly, S. J. Kent, A. K. Wheatley, *Expert Rev. Vaccines* **2019**, *18*, 269.
[2] C. Barnier-Quer, A. Elsharkawy, S. Romeijn, A. Kros, W. Jiskoot, *Pharmaceutics* **2013**, *5*, 392.
[3] C. Herzog, K. Hartmann, V. Künzi, O. Kürsteiner, R. Mischler, H. Lazar, R. Glück, *Vaccine* **2009**, *27*, 4381.
[4] M. Kanekiyo, C. J. Wei, H. M. Yassine, P. M. McTamney, J. C. Boyington, J. R. R. Whittle, S. S. Rao, W. P. Kong, L. Wang, G. J. Nabel, *Nature* **2013**, *499*, 102.
[5] H. M. Yassine, J. C. Boyington, P. M. McTamney, C. J. Wei, M. Kanekiyo, W. P. Kong, J. R. Gallagher, L. Wang, Y. Zhang, M. G. Joyce, D. Lingwood, S. M. Moin, H. Andersen, Y. Okuno, S. S. Rao, A. K. Harris, P. D. Kwong, J. R. Mascola, G. J. Nabel, B. S. Graham, *Nat. Med.* **2015**, *21*, 1065.
[6] C. Lee, J. Jeong, T. Lee, W. Zhang, L. Xu, J. E. Choi, J. H. Park, J. K. Song, S. Jang, C. Y. Eom, K. H. Shim, A. A. Seong Soo, Y. S. Kang, M. Kwak, H. J. Jeon, J. S. Go, Y. D. Suh, J. O. Jin, H. jong Paik, *Biomaterials* **2018**, *183*, 234.
[7] S. P. Kasturi, I. Skountzou, R. A. Albrecht, D. Koutsonanos, T. Hua, H. I. Nakaya, R. Ravindran, S. Stewart, M. Alam, M. Kwissa, F. Villinger, N. Murthy, J. Steel, J. Jacob, R. J. Hogan, A. García-Sastre, R. Compans, B. Pulendran, *Nature* **2011**, *470*, 543.
[8] W. Tao, H. S. Gill, *Vaccine* **2015**, *33*, 2307.
[9] C. Wang, W. Zhu, B. Z. Wang, *Int. J. Nanomed.* **2017**, *12*, 4747.
[10] V. Manolova, A. Flace, M. Bauer, K. Schwarz, P. Saudan, M. F. Bachmann, *Eur. J. Immunol.* **2008**, *38*, 1404.
[11] Y. N. Zhang, J. Lazarovits, W. Poon, B. Ouyang, L. N. M. Nguyen, B. R. Kingston, W. C. W. Chan, *Nano Lett.* **2019**, *19*, 7226.
[12] P. J. Tacken, I. S. Zeelenberg, L. J. Cruz, M. A. Van Hout-Kuijer, G. Van De Glind, R. G. Fokkink, A. J. A. Lambeck, C. G. Figdor, *Blood* **2011**, *118*, 6836.
[13] M. N. Vu, H. G. Kelly, A. K. Wheatley, S. Peng, E. H. Pilkington, N. A. Veldhuis, T. P. Davis, S. J. Kent, N. P. Truong, *Small* **2020**, *16*, 2002861.
[14] E. B. Puffer, J. K. Pontrello, J. J. Hollenbeck, J. A. Kink, L. L. Kiessling, *ACS Chem. Biol.* **2007**, *2*, 252.
[15] T. J. Moyer, A. C. Zmolek, D. J. Irvine, T. J. Moyer, A. C. Zmolek, D. J. Irvine, *J. Clin. Invest.* **2016**, *126*, 799.
[16] H. G. Kelly, H. X. Tan, J. A. Juno, R. Esterbauer, Y. Ju, W. Jiang, V. C. Wimmer, B. C. Duckworth, J. R. Groom, F. Caruso, M. Kanekiyo, S. J. Kent, A. K. Wheatley, *JCI Insight* **2020**, *5*.
[17] T. Tokatlian, D. W. Kulp, A. A. Mutafyan, C. A. Jones, S. Menis, E. Georgeson, M. Kubitz, M. H. Zhang, M. B. Melo, M. Silva, D. S. Yun, W. R. Schief, D. J. Irvine, *Sci. Rep.* **2018**, *8*, 16527.
[18] R. A. Schwendener, *Ther. Adv. Vaccines Immunother.* **2014**, *2*, 159.
[19] U. Bulbake, S. Doppalapudi, N. Kommineni, W. Khan, *Pharmaceutics* **2017**, *9*, 12.
[20] E. Kastner, R. Kaur, D. Lowry, B. Moghaddam, A. Wilkinson, Y. Perrie, *Int. J. Pharm.* **2014**, *477*, 361.
[21] A. Wagner, K. Vorauer-Uhl, *J. Drug Delivery* **2011**, *2011*, 591325.
[22] S. Sieber, M.-A. Shahbazi, M. Sedighi, J. Huwyler, F. Rahimi, A. H. Rezayan, D. Witzigmann, *Drug Delivery Transl. Res.* **2018**, *9*, 404.

[23] D. S. Watson, V. M. Platt, L. Cao, V. J. Venditto, F. C. Szoka, *Clin. Vaccine Immunol.* **2011**, *18*, 289.
[24] J. Guenaga, M. B. Zwick, J. Ingale, A. Stano, R. T. Wyatt, D. Nemazee, S. K. Sharma, *Cell Rep.* **2016**, *15*, 1986.
[25] H.-X. Tan, S. J. Kent, A. K. Wheatley, *J. Clin. Invest.* **2019**, *129*, 850.
[26] C. Dreyfus, N. S. Laursen, T. Kwaks, D. Zuijdgeest, R. Khayat, D. C. Ekiert, J. H. Lee, Z. Metlagel, M. V. Bujny, M. Jongeneelen, R. Van Der Vlugt, M. Lamrani, H. J. W. M. Korse, E. Geelen, Ö. Sahin, M. Sieuwerts, J. P. J. Brakenhoff, R. Vogels, O. T. W. Li, L. L. M. Poon, M. Peiris, W. Koudstaal, A. B. Ward, I. A. Wilson, J. Goudsmit, R. H. E. Friesen, *Science* **2012**, *337*, 1343.
[27] M. Kanekiyo, M. G. Joyce, R. A. Gillespie, J. R. Gallagher, S. F. Andrews, H. M. Yassine, A. K. Wheatley, B. E. Fisher, D. R. Ambrozak, A. Creanga, K. Leung, E. S. Yang, S. Boyoglu-Barnum, I. S. Georgiev, Y. Tsybovsky, M. S. Prabhakaran, H. Andersen, W.-P. Kong, U. Baxa, K. L. Zephir, J. E. Ledgerwood, R. A. Koup, P. D. Kwong, A. K. Harris, A. B. McDermott, J. R. Mascola, B. S. Graham, *Nat. Immunol.* **2019**, *20*, 362.
[28] W. C. Huang, S. Zhou, X. He, K. Chiem, M. T. Mabrouk, R. H. Nissly, I. M. Bird, M. Strauss, S. Sambhara, J. Ortega, E. A. Wohlfert, L. Martinez-Sobrido, S. V. Kuchipudi, B. A. Davidson, J. F. Lovell, *Adv. Mater.* **2020**, *32*, 2005637.
[29] S. W. Sauer, M. E. Keim, *Ann. Emerg. Med.* **2001**, *37*, 635.
[30] E. C. Cho, H. J. Lim, J. Shim, J. Kim, I. S. Chang, *Colloids Surf., A* **2007**, *299*, 160.
[31] D. Tarlinton, *Nature* **2014**, *509*, 573.
[32] W. Song, J. Craft, *Immunol. Rev.* **2019**, *288*, 85.
[33] M. A. Linterman, D. L. Hill, *F1000Research* **2016**, *5*, 88.
[34] W. Jiang, K. M. Wragg, H. X. Tan, H. G. Kelly, A. K. Wheatley, S. J. Kent, J. A. Juno, *J. Immunol. Methods* **2019**, *467*, 48.
[35] R. Wilson, G. Goebrecht, M. B. Zwick, R. T. Wyatt, A. Stano, S. Bale, J. Ingale, K. Tran, T. Ota, *J. Virol.* **2017**, *91*, e00443.
[36] Z. Chen, J. J. Moon, W. Cheng, *Bioconjugate Chem.* **2018**, *29*, 1251.
[37] K. T. Gause, A. K. Wheatley, J. Cui, Y. Yan, S. J. Kent, F. Caruso, *ACS Nano* **2017**, *11*, 54.
[38] S. Shao, J. Geng, H. Ah Yi, S. Gogia, S. Neelamegham, A. Jacobs, J. F. Lovell, *Nat. Chem.* **2015**, *7*, 438.
[39] C. Havenar-Daughton, D. G. Carnathan, A. V. Boopathy, A. A. Upadhyay, B. Murrell, S. M. Reiss, C. A. Enemuo, E. H. Gebru, Y. Choe, P. Dhadvai, F. Viviano, K. Kaushik, J. N. Bhiman, B. Briney, D. R. Burton, S. E. Bosinger, W. R. Schief, D. J. Irvine, G. Silvestri, S. Crotty, *Cell Rep.* **2019**, *29*, 1756.
[40] J. R. Francica, R. Laga, G. M. Lynn, G. Mužíková, L. Androvič, B. Aussedat, W. E. Walkowicz, K. Padhan, R. A. Ramirez-Valdez, R. Parks, S. D. Schmidt, B. J. Flynn, Y. Tsybovsky, G. B. E. Stewart-Jones, K. O. Saunders, F. Baharom, C. Petrovas, B. F. Haynes, R. A. Seder, *PLoS Biol.* **2019**, *17*, e3000328.
[41] D. J. Irvine, B. J. Read, *Curr. Opin. Immunol.* **2020**, *65*, 1.
[42] D. Gray, *Nat. Rev. Immunol.* **2002**, *2*, 60.
[43] T. E. Mandel, R. P. Phipps, A. P. Abbot, J. G. Tew, *Immunology* **1981**, *43*, 353.
[44] T. Tokatlian, B. J. Read, C. A. Jones, D. W. Kulp, S. Menis, J. Y. H. Chang, J. M. Steichen, S. Kumari, J. D. Allen, E. L. Dane, A. Liguori, M. Sangesland, D. Lingwood, M. Crispin, W. R. Schief, D. J. Irvine, *Science* **2019**, *363*, 649.
[45] J. J. Moon, H. Suh, A. V. Li, C. F. Ockenhouse, A. Yadava, D. J. Irvine, *Proc. Natl. Acad. Sci. U. S. A.* **2012**, *109*, 1080.
[46] P. J. M. Brouwer, A. Antanasijevic, Z. Berndsen, A. Yasmeen, B. Fiala, T. P. L. Bijl, I. Bontjer, J. B. Bale, W. Sheffler, J. D. Allen, A. Schorcht, J. A. Burger, M. Camacho, D. Ellis, C. A. Cottrell, A. J. Behrens, M. Catalano, I. del Moral-Sánchez, T. J. Ketas, C. LaBranche, M. J. van Gils, K. Sliepen, L. J. Stewart, M. Crispin, D. C. Montefiori, D. Baker, J. P. Moore, P. J. Klasse, A. B. Ward, N. P. King, R. W. Sanders, *Nat. Commun.* **2019**, *10*, 4272.
[47] V. V. Temchura, D. Kozlova, V. Sokolova, K. Überla, M. Epple, *Biomaterials* **2014**, *35*, 6098.
[48] V. Dubrovskaya, K. Tran, G. Ozorowski, J. Guenaga, R. Wilson, S. Bale, C. A. Cottrell, H. L. Turner, G. Seabright, S. O'Dell, J. L. Torres, L. Yang, Y. Feng, D. P. Leaman, N. Vázquez Bernat, T. Liban, M. Louder, K. McKee, R. T. Bailer, A. Movsesyan, N. A. Doria-Rose, M. Pancera, G. B. Karlsson Hedestam, M. B. Zwick, M. Crispin, J. R. Mascola, A. B. Ward, R. T. Wyatt, *Immunity* **2019**, *51*, 915.
[49] M. G. Brewer, A. DiPiazza, J. Acklin, C. Feng, A. J. Sant, S. Dewhurst, *Vaccine* **2017**, *35*, 774.
[50] M. C. Hanson, W. Abraham, M. P. Crespo, S. H. Chen, H. Liu, G. L. Szeto, M. Kim, E. L. Reinherz, D. J. Irvine, *Vaccine* **2015**, *33*, 861.
[51] R. A. Benson, M. K. L. Macleod, B. G. Hale, A. Patakas, P. Garside, J. M. Brewer, *eLife* **2015**, *4*, e06994.
[52] E. A. Thompson, S. Ols, K. Miura, K. Rausch, D. L. Narum, M. Spångberg, M. Juraska, U. Wille-Reece, A. Weiner, R. F. Howard, C. A. Long, P. E. Duffy, L. Johnston, C. P. O'Neil, K. Loré, *JCI Insight* **2018**, *3*, 120692.
[53] W. Liao, Z. Hua, C. Liu, L. Lin, R. Chen, B. Hou, *J. Immunol.* **2017**, *198*, 3846.